J Mater Sci: Mater Electron (2026) 37:855

Tailoring dielectric and optical properties of cholesteric liquid crystals via alkyl chain length modulation

Garima Chauhan[1], Ashwani Kumar Singh[2], Harsh Sharma[3], and Praveen Malik[3,*]

[1] *Department of Physics, School of Sciences (SOS), IFTM University, Moradabad, Uttar Pradesh 244102, India*
[2] *School of Engineering and Technology, IIMT University, Meerut, Uttar Pradesh 250001, India*
[3] *Liquid Crystal Research Lab, Department of Physics, Dr B R Ambedkar National Institute of Technology, Jalandhar, Punjab 144011, India*

Received: 14 January 2026
Accepted: 7 April 2026

ABSTRACT

Herein, we examined the effects of alkyl chain length variation on the optical and dielectric characteristics of cholesteric liquid crystals (ChLCs). Nematic liquid crystals with different alkyl chain lengths, 5CB, 7CB, and 8CB, were used with 5 wt% of chiral additive. The 7CB-based ChLC system exhibited an approximately 40% enhancement in permittivity relative to the 5CB counterpart. When the alkyl chain was extended to 8CB, the permittivity dropped by nearly 20% compared with that of the 5CB-based ChLC mixture. The electro-optical analysis indicates that the 7CB-based system exhibits the lowest threshold voltage of 2.2 V, demonstrating enhanced switching efficiency relative to 5CB (2.8 V) and 8CB (3.0 V) based ChLCs. Moreover, the photoluminescence studies demonstrated stronger emission intensity for 7CB incorporated ChLCs system. These results indicate the crucial role of alkyl chain length in modulating material behavior and identify 7CB as an optimal mesogen for achieving high-performance ChLCs systems. Such insights pave the way for designing tunable, energy-efficient materials for future-generation displays, sensors, and photonic devices.

1 Introduction

Cholesteric liquid crystals (ChLCs) have attracted considerable scientific attention due to its distinctive helical self-organization and wavelength-selective reflection characteristics [1–4]. The cholesteric phase is regarded as a distinct form of the nematic phase and is commonly known as chiral nematic liquid crystal [5–9]. The molecular organization in ChLCs consists of layers with the long molecular axes aligned parallel to the layer planes. Each successive plane is slightly rotated with respect to its neighboring layer [10–13]. The orientation vector of LCs molecules twists progressively along the layer axis until it completes a 360° rotation and returns to its initial direction. The distance over which this rotation occurs is known as pitch (p) [5, 14, 15]. Helical twisting power (HTP) of the ChLCs follows the relation: $HTP = 1/pc$. Here, c

Address correspondence to E-mail: malikp@nitj.ac.in

https://doi.org/10.1007/s10854-026-17230-y
Published online: 20 April 2026

indicates chiral dopant's amount [16–18]. The periodic helical shape allows them to reflect light that is circularly polarized and has the same handedness as the helix. The wavelength is dependent on optical pitch $\lambda = np$, represented by ChLCs have a distinctive helical shape. It gives them special optical characteristics such as rotating properties [8, 19], circular dichroism [4, 20], and selective light reflection [21, 22]. These characteristics make them valuable in various applications including display technologies, optical filters, sensors, and actuators [15, 23–42]. For electro-optical applications, a stable host nematic LCs mixture is an essential requirement and typically optimized to achieve the desired birefringence, dielectric anisotropy, viscosity, clearing point, and environmental stability.

Grey et al. synthesized optically active branched alkyl chain compounds that represented cholesteric nature. By shifting the position of the methyl group along one or both terminal alkyl chains and operating different molecular core groups, the changes in phase transition, cholesteric helix sense (handedness), and pitch length were noticed [43]. Vardayan et al. investigated the influence of gold nanoparticles (GNPs) upon room-temperature cyanobiphenyl (CB)-based nematic LCs (nCB, where $n = 5$, 6, 7, and 8) and revealed that GNPs doping significantly altered the nematic ordering, display characteristics, and mesophase stability in 5CB, 6CB, and 7CB. It was observed that both the concentrations of GNPs and the alkyl chain length of the CB molecular configuration affected the material properties [44]. Lim et al. explored the role of CB homologues in modifying the electro-optical characteristics of blue phases (BPs) and polymer-stabilized blue phases. The results demonstrated that incorporation of polymer stabilization improved driving voltage and switching hysteresis in ChLCs having nCB homologues. Furthermore, the electro-optical behavior of BPs was influenced by variations in alkyl chain length of nCB molecules in the ChLCs mixture. The rise time and Kerr coefficient showed noticeable changes with the alteration in chain length [46, 47]. Chirtoc et al. examined nCB ($n = 5$–8) compounds and demonstrated that with a mean critical exponent of $\beta = 0.241 \pm 0.012$, their nematic order parameter S(T) exhibit a nearly universal tricritical trend. They also highlighted the sensitivity of phase characteristics to slight structural changes by reporting a clear odd–even alternation in the impact of alkyl chain length [48]. The studies under review demonstrate that the stability, electro-optical characteristics, and phase transitions of LC systems are significantly influenced by the alkyl chain length of LCs [44–47]. Prior research has primarily focused on polymer-stabilized systems [46, 47, 49–51] or nanoparticle incorporation [44] but there is still a lack of systematic knowledge regarding how alkyl chain length regulates the dielectric and optical responses of chiral nematic-doped LCs. Moreover, achieving materials that simultaneously exhibit low threshold voltage and high optical response continues to be a major challenge in this field. Motivated by these findings, the present work investigates the interaction between alkyl chain length and chiral dopants. Table 1 summarizes key studies on cyanobiphenyl liquid crystal-based materials.

In this work, we are investigating the dielectric characteristics of three nematic LCs from the CB family (5CB, 7CB, and 8CB) with chiral dopant CB15, including permittivity (ε'), loss (ε''), ac conductivity (σ_{ac}), activation energy, relaxation frequency and electro-optical properties such as V-T characteristic,

Table 1 Representative studies on cyanobiphenyl liquid crystal-based materials

Reference	Material system	Key findings
Grey et al. [43]	Low-melting cholesterogenic biphenyl-nematic LC mixtures	Enabled room-temperature cholesteric thermochromism and electro-optical phase switching
Vardanyan et al. [44]	Au nanoparticle-doped nCB nematic LCs ($n = 5$–8)	Nanoparticle doping reduced threshold voltage and response time in 5CB–7CB systems
Lim et al. [45]	nCB-based blue phases and polymer-stabilized blue phases	Alkyl chain length-controlled driving voltage, hysteresis and Kerr response
Chirtoc et al. [47]	Pure nCB nematic LCs ($n = 5$–8)	Revealed quasi-tricritical nematic behavior with pronounced odd–even effects
Neha et al. [48]	Graphene quantum dot (GQDs) doped 5CB and 7CB nematic LCs	GQD incorporation enhanced dielectric response and lowered operating voltage

threshold voltage (V_{th}) and photoluminescence spectra (PL). These LCs exhibit variations in their molecular side chain length, denoted as C_nH_{2n-1}. The present study extends these insights to chiral systems by demonstrating how molecular structure and chirality together govern dielectric, electro-optical, and photoluminescence properties. The study provides a more comprehensive understanding of ChLCs for applications purpose such as smart windows and reflectors, which are not achievable in pure systems.

2 Material and methods

2.1 Materials

In the present work, commercial nematic LCs 5CB [Sigma-Aldrich (India)], 7CB [Sigma-Aldrich (India)], and 8CB [Tokyo Chemical Industry Pvt. Ltd (India)] were used. The chiral dopant CB15 was procured from Kingston Chemicals Company Ltd, UK. Each LC in this context possesses a distinctive molecular structure characterized by three key components: a flexible alkyl chain, a rigid cyclobenzene group, and a cyano group. Table 2 represents the chemical structure of LCs and the chiral dopant.

2.2 Preparation of planar-aligned LC cell

Two indium tin oxide (ITO)-coated transparent glass substrates with resistivity of $(10\Omega/cm^2)$ were employed to fabricate planar-aligned LC cells. At the first stage, the glass substrates were thoroughly washed with soap and subsequently rinsed with acetone. A polyamide solution was prepared through the dissolution of nylon (6/6) and m-cresol into methanol. In order to promote alignment, a solution of polyamide was applied using spin-coating at a speed of approximately 1000 rpm/min onto ITO glass substrates. Subsequently, the applied polyamide deposit was subjected to oven drying at a temperature of 120 °C for a duration of 1 h at a temperature of 50 °C [50, 51]. A unidirectional rubbing was applied on each side of ITO-coated substrates using velvet cloth. The substrates with the applied coating were enclosed, creating a sandwich structure having active area of 1 cm^2. A mylar spacer with a thickness of 6 μm is employed to form the gap between the two glass substrates, and a controlled mechanical load is applied during sealing to ensure uniform spacing and minimize thickness variations.

2.3 Preparation of ChLCs composites

Three samples were prepared, each containing a distinct LC: 5CB, 7CB, and 8CB. Chirality is introduced by

Table 2 Molecular structures of the utilized compounds

S. No	Compounds	Chemical structure
1	4-cyano-4′-pentylbiphenyl (5CB)	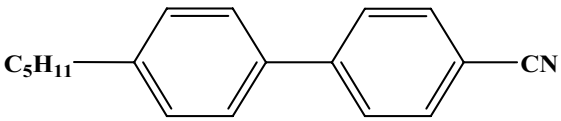 Cr (18 °C) N (35 °C) I
2	4′-heptyl-4-biphenylcarbonitrile (7CB)	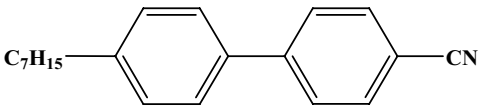 Cr(14.5 °C) N (42.8 °C) I
3	4′-n-octyl-4-cyanobiphenyl (8CB)	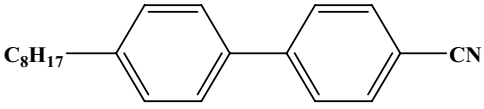 Cr (15 °C) SmA (33.5 °C) N (40.5 °C) I
4	(S)-4-(2-methylbutyl)-4′-cyanobiphenyl (CB15)	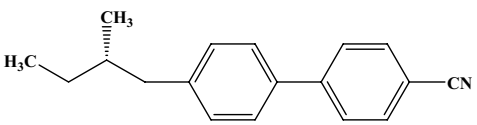

incorporating the chiral dopant CB15. These samples were designated as ChLCs-1, ChLCs-2 and ChLCs-3, respectively. For each mixture, the host LCs and CB15 were taken in a 95:5 ratio and mechanically stirred for one hour to achieve homogeneity. Further, the prepared mixtures were then heated until the isotropic phase was reached, after which they were filled into pre-aligned LC cells through capillary action.

2.4 Apparatus

The morphological and phase transitions study of prepared samples is conducted by utilizing a polarizing optical microscope (POM) (Nikon-LV100POL, Japan). For textures recording, a charge-coupled camera (Q-28378) is integrated with POM. Temperature-dependent investigations of the samples were conducted by subjecting sample cells to controlled heating and freezing conditions by a hotstage (Linkam-THMS600E, UK), coupled with a temperature controller (Linkam T-95, UK) with accuracy of ± 0.01 K. The entire setup is comprehensively outfitted and interfaced with Linksys software. Dielectric investigations were also carried out using an impedance analyzer (Wayne Kerr 6500B, UK) within the frequency range (20 Hz–10 MHz), which has a measurement accuracy of ± 0.05%. For the assessment of electro-optical properties, a helium neon laser (Melles Griot, USA) with a power of 5 mW and a wavelength of 632.8 nm was operated as the light source. In the optical measurements, the LCs cell was positioned in a crossed configuration between the polarizer and analyzer. A square/triangular waveform was applied across the LCs cell (active area = 1 cm^2) through a function generator (Tektronix-AFG3021B, USA). The response of the LCs sample was recorded by a photo-detector (Instec PD-02, USA) connected to a digital multimeter (Keysight-34465A, USA). The voltage-dependent morphological studies in the range of 0–50 V were carried out across the LC cell using a function generator in AC mode. The voltage was directly applied to the cell with an active area of 1 cm^2, and corresponding POM textures were recorded at discrete applied voltages. PL was also examined using a fluorescence spectrophotometer (Cary Eclipse, Agilent Technologies, USA).

3 Results and discussion

3.1 Morphological studies

The morphological studies of ChLCs-1 composites in the presence of applied voltage are shown in Fig. 1a–f. At 0 V, the LCs molecules are in the chiral phase as shown in Fig. 1a. As the voltage increases, the morphology of the sample undergoes a significant transformation. At 40 V (Fig. 1e), filament-type morphologies were observed. The pattern originates from the helical arrangement of the director, with dark lines appearing whenever the local director is oriented parallel to the light propagation direction. On further increasing the voltage, i.e., at 50 V as shown in Fig. 1f, LCs molecules align in the direction of the applied field. The dark pattern, as shown in Fig. 1f, demonstrates that the local director is aligned along the direction of propagation of light. This change is attributed to the increased dielectric torque aligning the LCs molecules more uniformly along the field direction, thereby disrupting the initial filamentary texture and promoting a more field-aligned structure. Figure 2 exhibits the morphology of ChLCs-2 composites under the application of an electric field. Figure 2a shows the oily streaks or Grandjean texture. The helical axis of the LCs phase is oriented along the direction of propagation of light. It is also called Grandjean orientation [52]. On applying the electric field, the Grandjean texture disappears owing to distortion of the helical configuration. At 50 V (Fig. 2f), LCs molecules completely distorted the cholesteric phase and a dark appearance is shown under POM. In the present study, the observed textures of ChLCs-3 correspond to a cholesteric phase (Fig. 3a). However, well-defined fingerprint or Grandjean textures are not obtained in the 8CB-based system. This behavior can be attributed to the presence of smectic-A (SmA) ordering in 8CB, which is inherent to the pure system. These smectic fluctuations hinder efficient chiral twist induction by the dopant, thereby suppressing the formation of a stable and well-defined helical structure. With increasing voltage (particularly above ~ 20–30 V, Fig. 3c–e), these periodic features gradually disappear and the texture becomes uniformly dark under crossed polarizers, indicating that helical twist has been suppressed and the director tries to reorient perpendicular to the substrates (homeotropic state). This loss of birefringent domains and shift to extinction are a standard optical signature of complete or near-complete helix

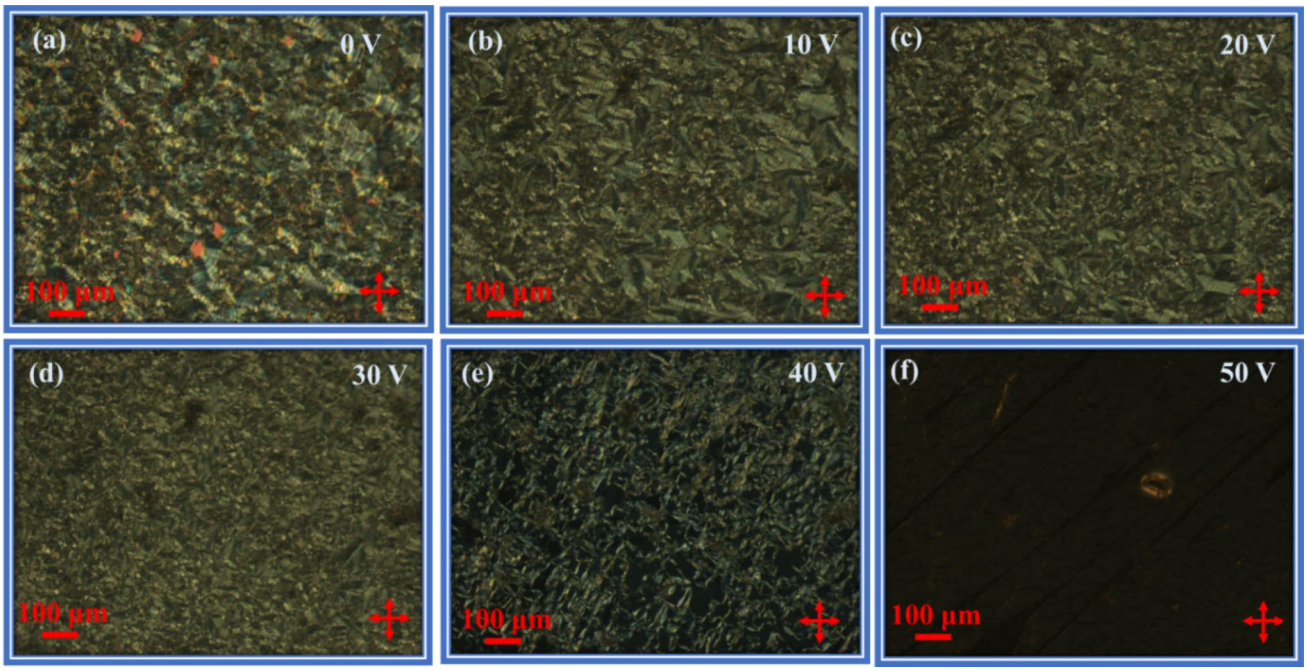

Fig. 1 Voltage-dependent morphology of ChLCs-1 composites at **a** 0 V, **b** 10 V, **c** 20 V, **d** 30 V, **e** 40 V, and **f** 50 V

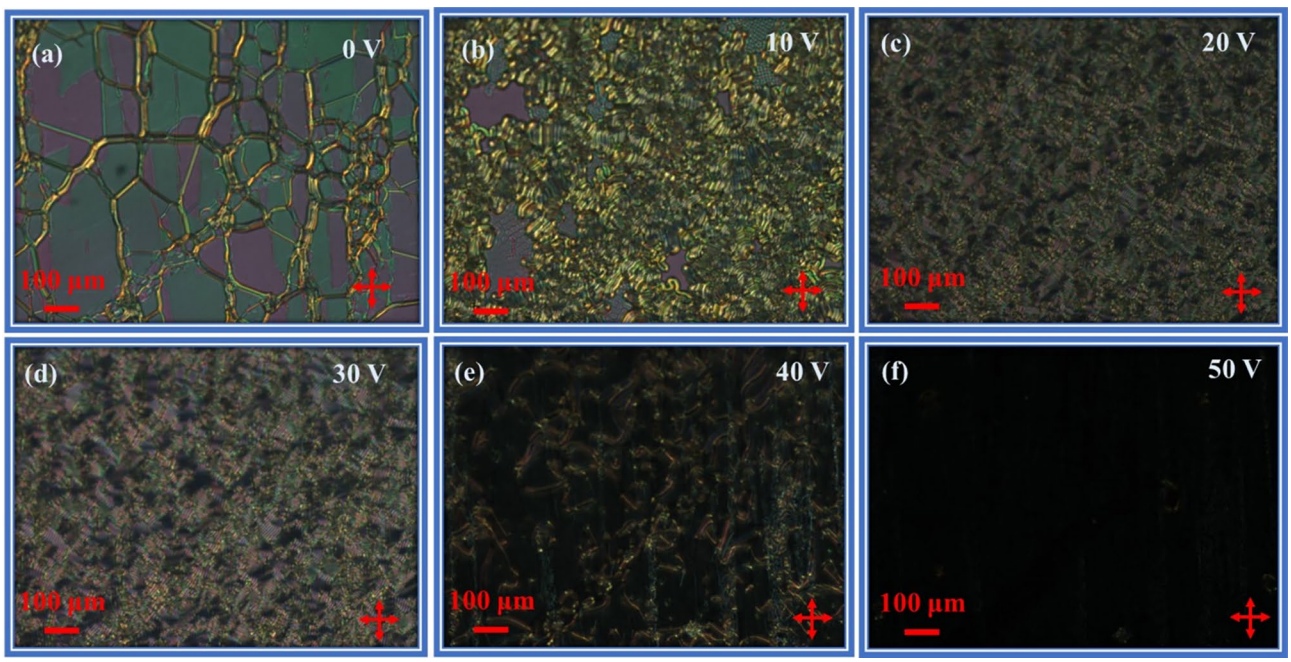

Fig. 2 Voltage-dependent morphology of ChLCs-2 at **a** 0 V, **b** 10 V, **c** 20 V, **d** 30 V, **e** 40 V, and **f** 50 V

unwinding in cholesteric systems. The superior homeotropic alignment (Fig. 2f) in the 7CB-based composite (ChLCs-2) arises from its stable cholesteric phase and balanced intermolecular interactions which provide moderate elastic resistance and allow efficient helix unwinding at lower voltages. In contrast, the 5CB-based system (ChLCs-1), due to its shorter alkyl chain length, exhibits weaker intermolecular interactions,

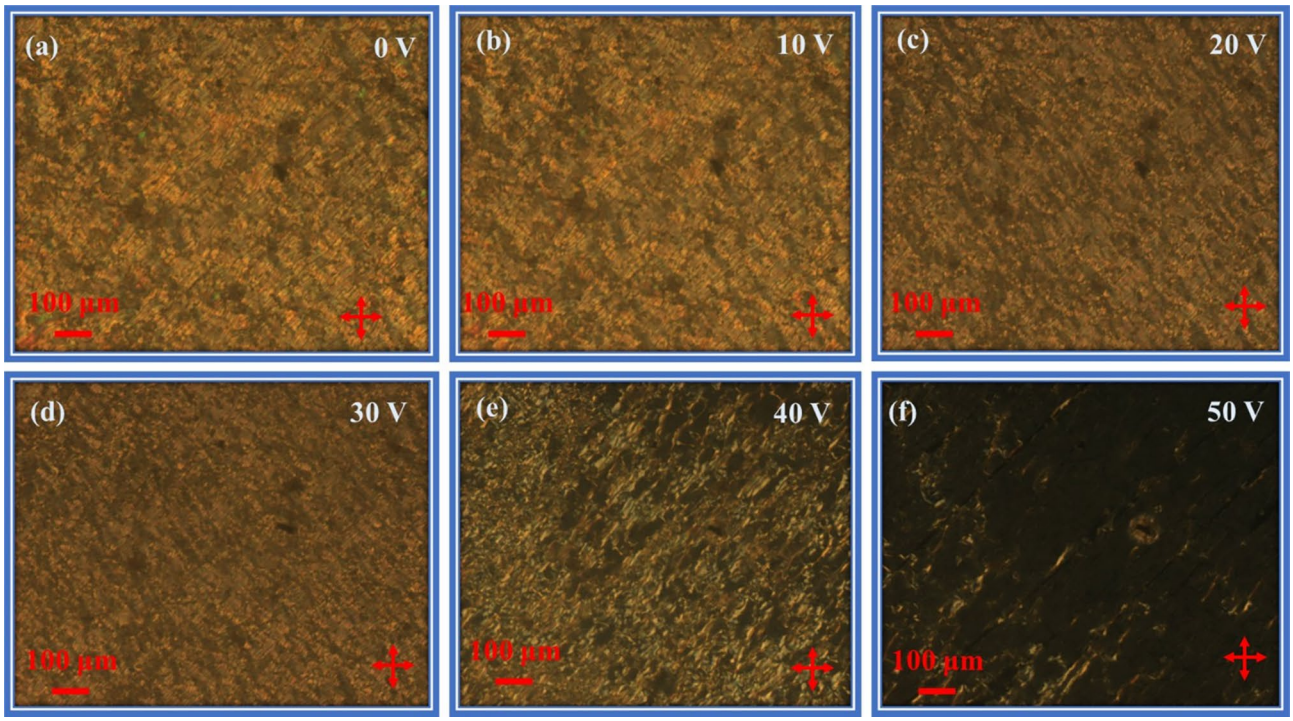

Fig. 3 Voltage-dependent morphology of ChLCs-3 at **a** 0 V, **b** 10 V, **c** 20 V, **d** 30 V, **e** 40 V, and **f** 50 V

leading to reduced cooperative reorientation and less efficient alignment as shown in Fig. 1f. However, the behavior of the ChLCs-3 system can be understood from the proximity of 8CB to the SmA phase. These short-range layered correlations increase the elastic rigidity of the system, particularly the twist (K_{22}) and bend (K_{33}) elastic constants. Consequently, the applied electric field of 50 V (Fig. 3f) is insufficient to completely overcome this elastic resistance, leading to incomplete unwinding of the helical structure in the ChLCs-3 system. The morphological comparison of 5CB, 7CB, and 8CB-based chiral system reveals that both the length of the alkyl chain and molecular polarity strongly influence the resulting textures. 7CB-based ChLCs-2 composites achieve a balance between cholesteric phase stability and field-induced molecular reorientation. These findings emphasize that the combined effects of chain length, dipole strength, and dielectric torque govern the field-induced morphological transitions in ChLCs composites.

Figure 4 shows the temperature-dependent morphological studies of ChLCs-1, ChLCs-2, and ChLCs-3 composites. As the temperature rises, the well-defined cholesteric patterns gradually fade and eventually disappear, indicating a transition to the isotropic phase where no birefringence is visible under POM. ChLCs-1 reaches a completely isotropic state at around 31 °C, while ChLCs-2 and ChLCs-3 do so at higher temperatures of 39.5 and 37.5 °C, respectively. These differences in clearing temperatures from the pure system show that adding the chiral dopant directly affects the thermal stability of the liquid crystalline phase. It suggests that the dopant slightly disturbs the molecular arrangement of the host, reducing the degree of order and facilitating the transition to the isotropic phase at a lower temperature.

3.2 Dielectric parameters

The dielectric characteristics of LCs are remarkably responsive to their molecular composition, alignment geometry, and structural alterations induced by dopants.

The real component of the ε' is expressed in Eq. (1) [53–56]:

$$\varepsilon'(\omega) = \varepsilon(\infty) + \frac{\varepsilon(0) - \varepsilon(\infty)}{1 + (\omega\tau)^2} \quad (1)$$

The imaginary component of ε'' is expressed in Eq. (2):

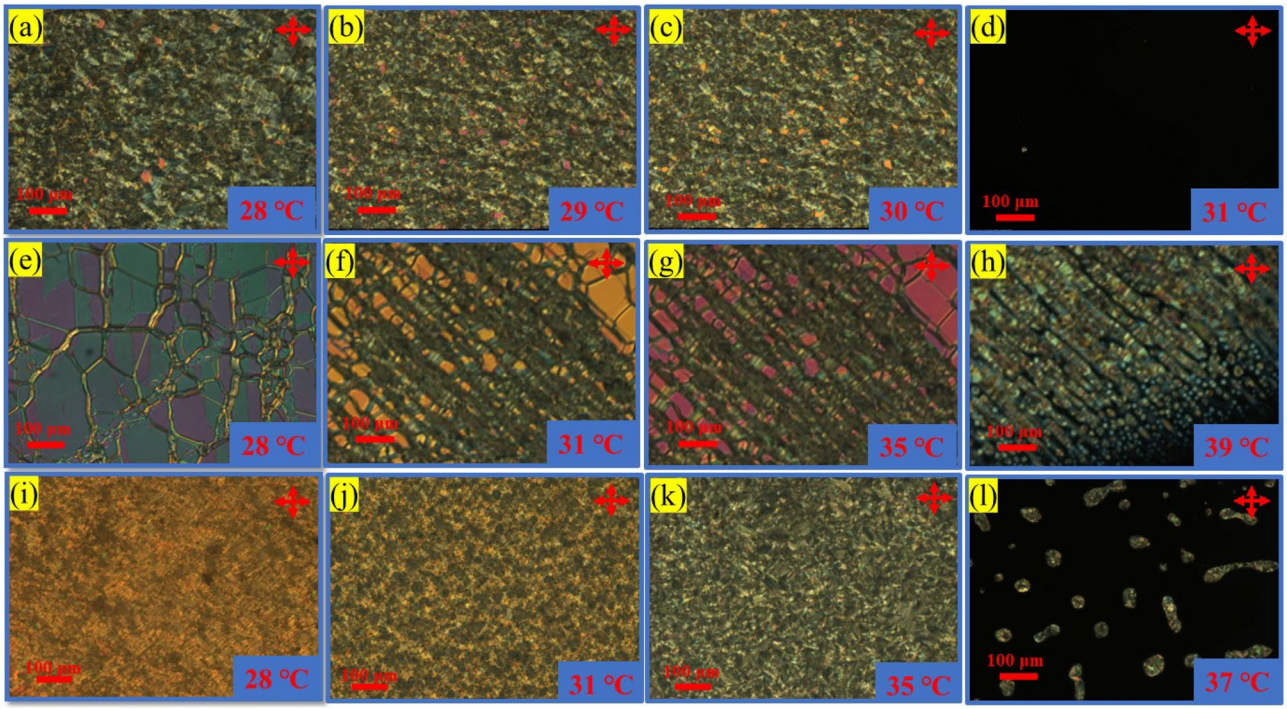

Fig. 4 Temperature-dependent POM textures of **a–d** ChLCs-1, **e–h** ChLCs-2, and **i–l** ChLCs-3 composites at different temperatures, showing the gradual transition from cholesteric to isotropic phase with increasing temperature

$$\varepsilon''(\omega) = (\varepsilon(0) - \varepsilon(\infty))\frac{\omega\tau}{\left[1 + (\omega\tau)^2\right]} \tag{2}$$

The generalized frequency-dependent expression for complex dielectric permittivity $\varepsilon^*(\omega)$ (Eq. 3) is mathematically expressed as

$$\varepsilon^*(\omega) = \varepsilon(\infty) + \sum_i \frac{\delta\varepsilon_i}{1 + \left(j\omega\tau_i\right)^{(1-\alpha_i)}} \tag{3}$$

In this expression, τ stands for the relaxation time associated with given dielectric relaxation process and ω refers to angular frequency of applied alternating field. Here, $\varepsilon(0)$ and $\varepsilon(\infty)$ refer to the dielectric permittivity measured at the limiting low and high frequencies, respectively.

Figure 5 represents comparative analysis of ε' for various alkyl chain lengths, highlighting the effect of structural diversity on dielectric properties. The observed value found for composites ChLCs-1, ChLCs-2, and ChLCs-3 is 2, 2.8, and 1.6, respectively, at 1 kHz and at 28 °C. In ChLCs-1, the shorter 5CB chains limit molecular elongation, slightly reducing orientational order and dipole alignment efficiency that leads to moderate dielectric response.

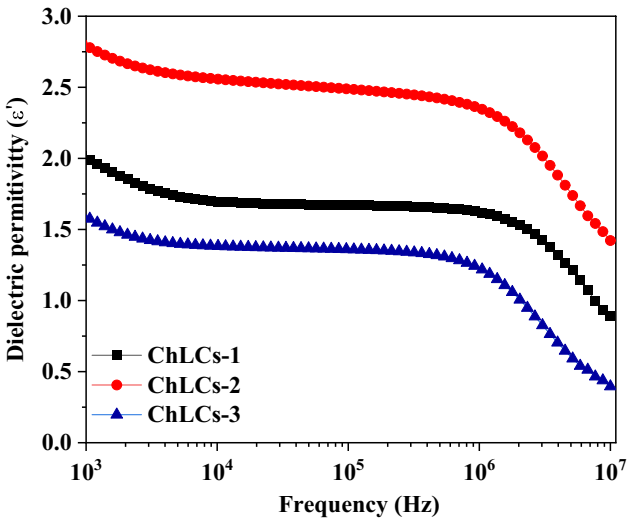

Fig. 5 Dielectric permittivity of ChLCs-1, ChLCs-2, and ChLCs-3 composites at 28 °C

In ChLCs-2, 7CB has an intermediate alkyl chain length which provides a balanced molecular aspect ratio. This balance enhances orientational order in the cholesteric phase and allows stable alignment of molecular dipoles. As a result, ChLCs-2 exhibits the

highest ε' which reflects efficient dipole alignment and stronger polarization under the applied electric field.

In contrast, ChLCs-3 exhibits the lowest permittivity among the three composites. This reduction may be attributed to the presence of antiparallel correlations between cyano groups in 8CB. Such antiparallel interactions reduce the net dipole contribution, thereby limiting the response of molecular dipoles to the applied electric field [57–59].

Figure 6 illustrates ε'' spectra of three distinct composites ChLCs-1, ChLCs-2, and ChLCs-3 at varying frequencies and at temperature of 28 °C. The observed value of ε'' composites ChLCs -1, ChLCs-2 and ChLCs-3 is 2.44, 1.85, and 1.28, respectively, at 1 kHz. The behavior of the LCs cell at low frequencies (~ 1 kHz) for all the composites is dominated by the movement of ions that lead to a specific dielectric relaxation process. The explanation provides insights into the dynamics of polarization and ionic drift within the material when the applied electric field is present. At higher frequency, all the composites exhibit second relaxation which might be attributed to relaxation of molecules along their short axis [30, 60]. A clear reduction in ε'' is evident in ChLCs-3 when compared to those containing ChLCs-1 and ChLCs-2. This can be attributed to the distinct structural characteristics of 8CB which possess longer alkyl chain. In this phase, the molecules are organized in layers which significantly restricts their rotational motion. It also hinders the realignment of dipoles in response to an external electric field. As a result, energy dissipation through dipolar relaxation is minimized. Moreover, the enhanced molecular ordering may limit the movement of ionic impurities, thereby reducing conductive losses. Together, these factors contribute to the overall decrease in dielectric loss which appears to stem more from constrained polarization processes. Furthermore, at higher frequency in (~ 3 MHz), the shift toward lower frequencies in the loss peak of ChLCs-3 composites compared to ChLCs-1 and ChLCs-2 suggests that the relaxation processes of 8CB occur at a slower rate.

Figure 7 shows frequency-dependent σ_{ac} of composites ChLCs-1, ChLCs-2, and ChLCs-3. The frequency-dependent σ_{ac} exhibits distinct trends across different frequency ranges. In the lower-frequency range (1 kHz), ChLCs-1 displays the highest σ_{ac} followed by ChLCs-2 and then ChLCs-3. This trend can be attributed to molecular structure and chain length of the LC compounds. The shorter alkyl chain in LCs 5CB leads to less molecular rigidity and tighter packing, allowing greater ionic mobility and thus enhanced conductivity. In contrast, 8CB with longest alkyl chain exhibits restricted ionic motion due to comparatively high viscosity. At higher frequency domain (~ 3–10 MHz), ChLCs-2 doped with 7CB demonstrates highest σ_{ac} among the three. This shift is associated with dipolar relaxation and dielectric response of LCs molecules under high-frequency fields. The molecular structure of 7CB, with its intermediate alkyl chain length, supports efficient dipole reorientation. Consequently, ChLCs-2 shows enhanced

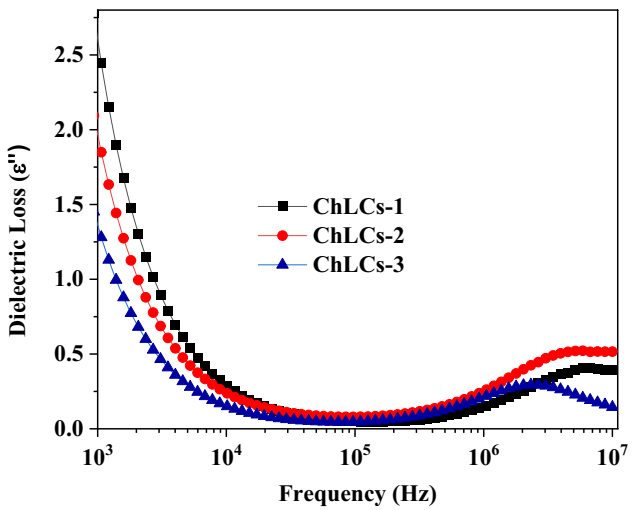

Fig. 6 Frequency-dependent dielectric loss of ChLCs-1, ChLCs-2, and ChLCs-3 composites at 28 °C

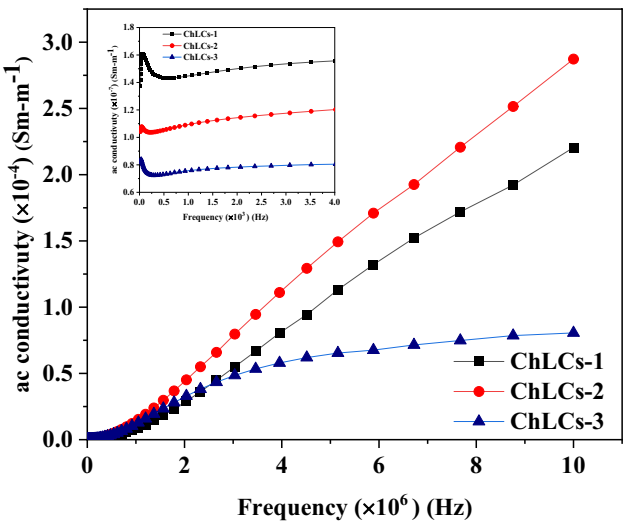

Fig. 7 Frequency-dependent AC conductivity of ChLCs-1, ChLCs-2, and ChLCs-3 composites

σ_{ac} at higher frequencies compared to ChLCs-1 and ChLCs-3 these are less responsive in this regime due to less favorable molecular mobility and intermolecular interactions.

The frequency-dependent total conductivity is defined by Jonscher's power law, Eq. (4):

$$\sigma(f) = \sigma_{i/dc} + Af^{P} \tag{4}$$

where A is a constant and P is a fractional exponential constant. The value of P lies between 0 and 1. $\sigma_{i/dc}$ corresponds to the ionic or DC conductivity of the system. Figure 8a illustrates the frequency-dependent total conductivity σ, calculated using Eq. (4). In the low-frequency region, i.e., < 1 kHz, Af^{P} component of Eq. (4) is negligible and therefore conductivity depends on the first part of Eq. (4), i.e., ionic part. The value of $\sigma_{i/dc}$ was found to be 1.570×10^{-7}, 9.9453×10^{-8}, and 7.56119×10^{-8} S/m for ChLCs-1, ChLCs-2, and ChLCs-3, respectively. $\sigma_{i/dc}$ versus inverse of temperature ($^{1}/_{T}$) has been plotted in Fig. 8b and linear fitting was performed to satisfy the Arrhenius Eq. (5): [61, 62]

$$\ln(\sigma_i) = \ln(\sigma_0) - {}^{E_a}/_{K_b T} \tag{5}$$

where σ_0 is the pre-exponential factor, E_a is the activation energy, K_b is the Boltzmann constant, and T is the temperature. The E_a was calculated by slopes of $\ln(\sigma_i)$ versus $^{1}/_{T}$ graph, and the values of E_a are 0.212, 0.244, and 0.236 eV for for ChLCs-1, ChLCs-2, and ChLCs-3, respectively.

The Cole–Cole analysis provides detailed insight into the relaxation behavior of the studied composites.

The dielectric strength $\delta\varepsilon = \varepsilon_s - \varepsilon_\infty$, where ε_s and ε_∞ are the permittivity values at low and high frequencies, respectively, of each composite was obtained from the Cole–Cole plots with ε_s and ε_∞ values extracted from the high and low frequency limits as illustrated in the inset of Fig. 9. These plots reveal the extent of deviation from ideal Debye behavior and provide quantitative information on the relaxation dynamics and heterogeneity of the investigated LCs composites [63]. $\delta\varepsilon$ is obtained as 1.24, 1.69, and 1.09 for ChLCs-1, ChLCs-2, and ChLCs-3, respectively. These values indicate that ChLCs-2 exhibits the strongest dipolar response. The relaxation frequencies f_r of the investigated composites obtained from the maximum of ε'' in the Cole–Cole plots were found to be 6.7, 5.8, and 2.6 MHz for ChLCs-1, ChLCs-2, and ChLCs-3, respectively. The relaxation times (τ) of the investigated composites were calculated from the peak of the ε'' using the relation: $(\tau) = 1/(2\pi f_r)$. For ChLCs-1, the relaxation time was found to be approximately 2.37×10^{-8} s. For ChLCs-2, τ is slightly higher at 2.74×10^{-8} s, while ChLCs-3 exhibits the longest relaxation time of 6.12×10^{-8} s, reflecting slower dipolar reorientation due to longer alkyl chains and associated molecular interactions.

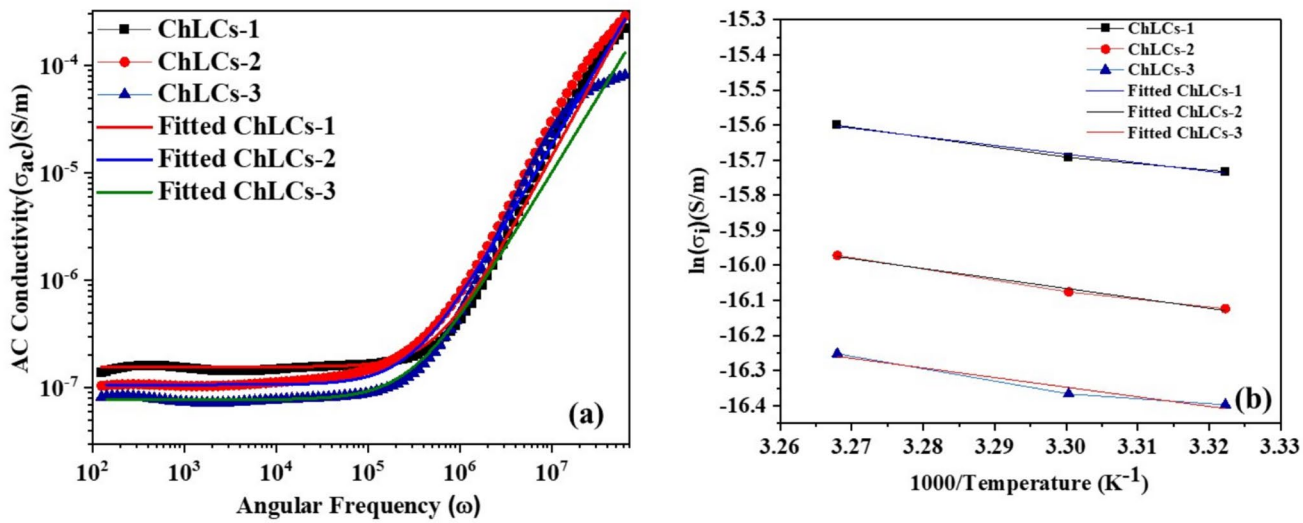

Fig. 8 **a** Angular frequency-dependent AC conductivity and **b** Arrhenius plot of $\ln(\sigma_i)$ versus 1000/T for ChLCs-1, ChLCs-2, and ChLCs-3 composites along with corresponding linear fits

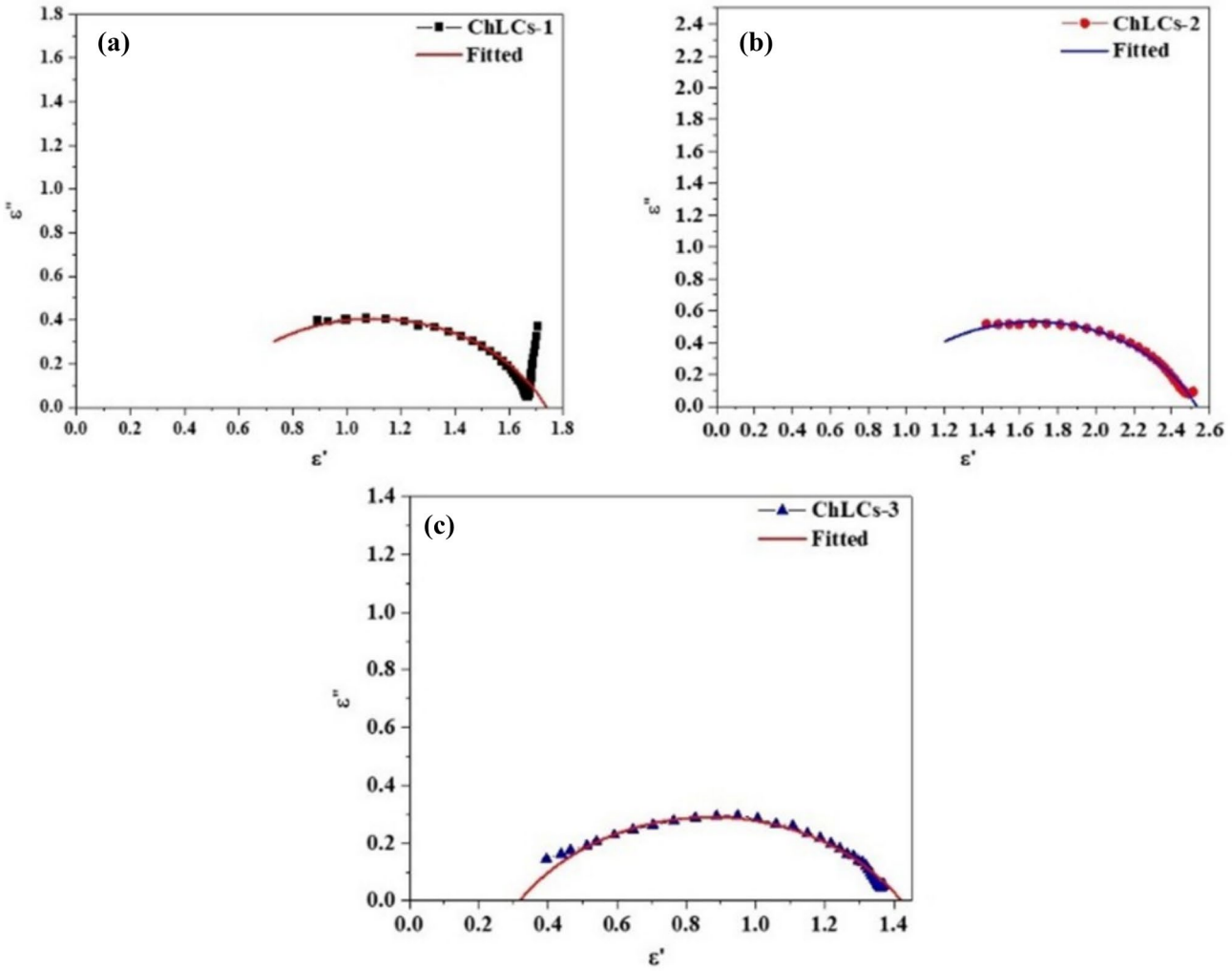

Fig. 9 Cole–Cole plot of **a** ChLCs-1, **b** ChLCs-2, and **c** ChLCs-3 composites along with corresponding fitted lines at 28 °C

3.3 Electro-optical studies

A photodetector coupled with a digital multimeter was employed to record the transmitted light intensity from the LC cells. A function generator supplied a sinusoidal AC voltage (frequency typically 1 kHz) across the cell, ramped from 0 V to a maximum value (20 V) in steps of 0.1 V. Measurements were intentionally limited to 0–20 V AC (1 kHz) because the objective here is solely the precise determination of the V_{th} for the onset of director reorientation. Figure 10 illustrates the voltage-dependent (*V*–*T*) transmittance of ChLCs-1, ChLCs-2, and ChLCs-3 composites. The presence of a chiral dopant also influences the *V*-*T* characteristics. Initially, the molecules in all these composites are in a chiral configuration. As the applied voltage increases, the molecules respond by attempting to align themselves with the direction of the applied electric field. In Fig. 10, when no voltage is applied, ChLCs cells show maximum transmittance because the helical structure turns the polarized light so that it can pass through the crossed position of polarizer and analyzer. Upon application of an electric field, the LCs' orientation changes from planar to homeotropic state of alignment. This shows that light remains parallel to the first polarizer and consequently blocked by the crossed analyzer, leading to a rapid decrease in transmittance for ChLCs cells. From the experimental data as shown in Fig. 10a, b and c, V_{th} is obtained 2.8, 2.2 and 3.0 V for ChLCs-1, ChLCs-2,

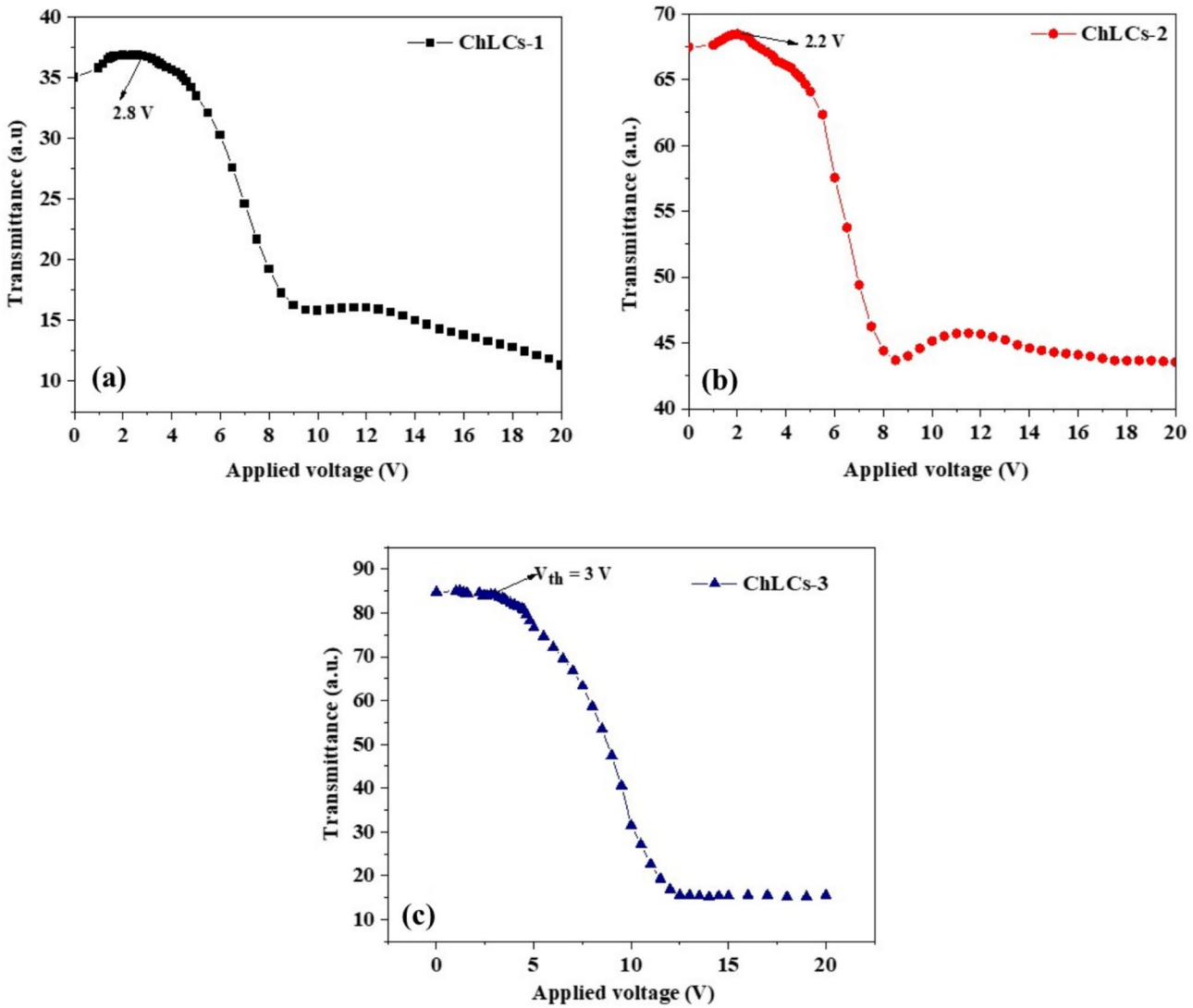

Fig. 10 Voltage-transmittance characteristics of **a** ChLCs-1, **b** ChLCs-2, and **c** ChLCs-3 composites at 28 °C

and ChLCs-3, respectively. These variations may be arisen due to difference in alkyl chain length, shorter chains (5CB) enhance molecular mobility but may increase elastic resistance due to higher bend elastic constants while intermediate lengths (7CB) optimize dielectric coupling and reduce viscosity, leading to the lowest V_{th}. Longer chains (8CB) introduce steric hindrance and greater rotational viscosity, requiring higher voltages to achieve reorientation due to reduced effective $\Delta\epsilon$ and increased energy barriers for helix unwinding [64].

3.4 Photoluminescence studies

PL emission spectra were recorded at an excitation wavelength of 300 nm (slit width 5 nm) as shown in Fig. 11. Before measuring the PL of all three composites, control measurements were performed on bare ITO cells and aligned cells without LCs. These showed negligible emission, confirming that the observed PL originates only from the three LC composites. Therefore, the enhanced PL intensity is solely due to the LCs composites themselves. All samples exhibit an emission peak centered around ~ 395 nm, which can be attributed to intrinsic π–π^* electronic transitions of the cyanobiphenyl core that originates from the

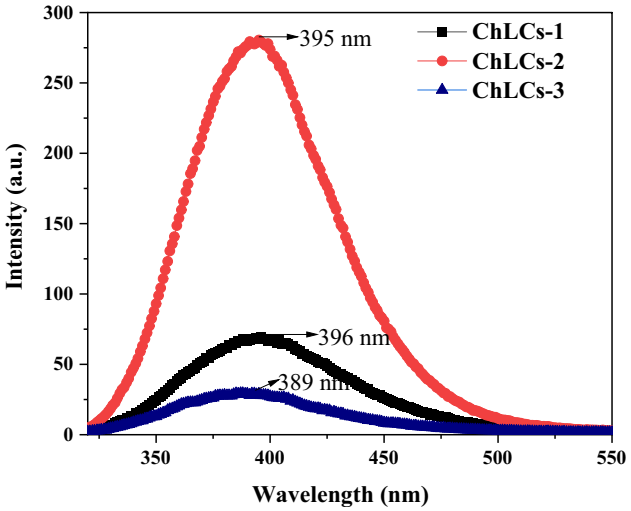

Fig. 11 Photoluminescence spectra of ChLCs-1, ChLCs-2, and ChLCs-3 composites at 28 °C

excited singlet state of the conjugated biphenyl system [65]. Typically, nCB compounds exhibit strong absorption in the UV region (~ 280–320 nm) [66]. Therefore, an excitation wavelength of 300 nm was selected to ensure efficient excitation of these electronic states and to obtain a strong PL response.

The intrinsic molecular emission, contributions from defect-assisted emission (due to local disorder, domain boundaries, or impurities) and aggregation-induced effects (such as excimer-like states) may also influence the observed PL intensity as reported in cyanobiphenyl-based LCs systems [67]. Since no significant shift in emission peak position (~ 389–396 nm) is observed, aggregation-related emission, such as excimer formation is unlikely in the present system.

Although all samples exhibit similar emission peak positions, a variation in PL intensity is observed among the composites. The highest intensity is obtained for ChLCs-2 (7CB-based system), followed by ChLCs-1 and ChLCs-3. The enhanced PL intensity in ChLCs-2 may be correlated with its well-defined Grandjean (oily streak) texture (Fig. 1a), indicating a uniformly aligned helical structure. Such ordering can reduce non-radiative decay pathways associated with structural defects and improve emission efficiency. However, it is important to note that texture alone does not determine PL behavior. The observed variation in PL intensity likely arises from a combination of molecular packing, defect density and intermolecular interactions. In particular, the possibility of changes in internal quantum efficiency due to molecular packing cannot be ruled out. The molecular arrangement in 7CB may facilitate more efficient radiative recombination, consistent with observations in similar cyanobiphenyl and organic molecular systems where molecular stacking and phase-dependent packing modulate PL quantum efficiency [68].

In ChLCs-1 (5CB-based system), the shorter alkyl chain reduces long-range molecular ordering, leading to relatively higher disorder and increased non-radiative relaxation pathways, resulting in moderate PL intensity. In contrast, ChLCs-3 (8CB-based system) shows reduced PL intensity, which may be due to disruption of the cholesteric helical structure, influencing light propagation and emission extraction through modification of the photonic bandgap. Table 3 represents dielectric and electro-optical properties of ChLCs-1, ChLCs-2, and ChLCs-3.

4 Conclusion

In this study, cholesteric liquid crystal composites were prepared using LCs with varying alkyl chain lengths of LCs (5CB, 7CB, and 8CB) in combination with the chiral dopant (S)-4-(2-methylbutyl)-4′-cyanobiphenyl. The voltage-dependent morphological and electro-optical studies revealed that the alkyl chain length significantly influences the molecular organization and functional behavior of ChLCs. Among the studied systems, 7CB-based composites (ChLCs-2) exhibited superior alignment in the homeotropic state at lower voltages, higher permittivity (2.8),

Table 3 Dielectric and electro-optical properties of composites ChLCs-1, ChLCs-2, and ChLCs-3

Composites	ε'	ε''	f_r(MHz)	$\tau \times 10^{-8}$ (sec)	V_{th}(V)	PL intensity (a.u.)
ChLCs-1	2.0	2.4	6.7	2.37	2.8	69
ChLCs-2	2.8	1.8	5.8	2.74	2.2	280
ChLCs-3	1.6	1.2	2.6	6.12	3.0	29

enhanced photoluminescence with an intensity of 280 au, and reduced threshold voltage (2.2 V) compared to the 5CB and 8CB LC counterparts. These results underscore the significance of optimizing molecular chain length for enhancing the electro-optical properties of ChLCs. The findings not only advance the fundamental understanding of the structure–property relationship in liquid crystalline systems but also open pathways for the development of energy-efficient ChLCs-based devices such as smart windows, reflective displays, tunable photonic elements, and low-power optical modulators. The tunability offered by molecular structure provides a versatile platform for next-generation optoelectronic applications.

Acknowledgements

The authors would grateful to Dr. B R Ambedkar National Institute of Technology Jalandhar, Punjab, India for laboratory facilities. The authors are also thankful to the DST project (CRG/2022/007362).

Author contributions

Material preparation, experiments, data analysis, and manuscript drafting were carried out by Garima Chauhan. Harsh Sharma and Ashwani Kumar Singh contributed to methodology and investigation. Praveen Malik supervised the work and contributed to validation and manuscript review and editing. All authors read and approved the final manuscript.

Funding

The authors declare that no funds, grants, or other support were received during the preparation of this manuscript.

Data availability

The data that support the findings of this study are available from the corresponding author upon reasonable request.

Declarations

Competing Interest The authors declare no competing interests.

References

1. N. Tamaoki, Cholesteric liquid crystals for color information technology. Adv. Mater. **13**(15), 1135–1147 (2001)
2. H. Zhou, H. Wang, W. He, Z. Yang, H. Cao, D. Wang, Y. Li, Research progress of cholesteric liquid crystals with broadband reflection. Molecules **27**, 14 (2022). https://doi.org/10.3390/molecules27144427
3. P.S. Salter, G. Carbone, S.A. Jewell, S.J. Elston, P. Raynes, Unwinding of the uniform lying helix structure in cholesteric liquid crystals. Phys. Rev. E **80**(9), 041707 (2009). https://doi.org/10.1103/PhysRevE.80.041707
4. F.D. Saeva, J.J. Wysocki, Induced circular dichroism in cholesteric liquid crystals. J. Am. Chem. Soc. **93**(22), 5928–5929 (1971)
5. D. Coates, Development and applications of cholesteric liquid crystals. Liq. Cryst. **42**(5), 653–665 (2015). https://doi.org/10.1080/02678292.2015.1020454
6. S. Chandrasekhar, Cholesteric liquid crystals, in *Polymeric Liquid Crystals and Low-Dimensional Solids*. (Springer, 1984), pp.213–220. https://doi.org/10.1007/978-1-4613-2367-9_9
7. M. Mitov, N. Dessaud, Going beyond the reflectance limit of cholesteric liquid crystals. Nat. Mater. **5**(5), 361–364 (2006). https://doi.org/10.1038/nmat1619
8. G.W. Day, O.L. Gaddy, Electric-field-induced optical rotation in cholesteric liquid crystals. Proc. IEEE **56**(6), 1113–1114 (1968). https://doi.org/10.1109/PROC.1968.6482
9. M. Mitov, Cholesteric liquid crystals with a broad light reflection band. Adv. Mater. **24**, 6260–6276 (2012). https://doi.org/10.1002/adma.201202913
10. A. Boudet, C. Binet, M. Mitov, C. Bourgerette, E. Boucher, Microstructure of variable pitch cholesteric films and optical properties. Eur. Phys. J. E **2**, 247–253 (2000). https://doi.org/10.1007/PL00013671
11. N.Y. Ha, Y. Ohtsuka, S.M. Jeong, Y. Takanishi, K. Ishikawa, H. Takezoe, Fabrication of a simultaneous red–green–blue reflector using single-pitched cholesteric liquid crystals. Nat. Mater. **7**(1), 43–47 (2008). https://doi.org/10.1038/nmat2045
12. H.K. Bisoyi, T.J. Bunning, Q. Li, Stimuli-driven control of the helical axis of self-organized soft helical superstructures. Adv. Mater. **30**, 1706512 (2018). https://doi.org/10.1002/adma.201706512

13. T.H. Kao, H.H. Hsu, J.J. Chen, L.R. Lee, H.Y. Chen, J.T. Chen, Fabrication of polymer/cholesteric liquid crystal films and fibers using nonsolvent-induced phase separation method. Langmuir **40**(27), 14166–14172 (2024). https://doi.org/10.1021/acs.langmuir.4c01759
14. D.A. Dunmur, M.R. Manterfield, W.H. Miller, J.K. Dunleavy, Dielectric and optical properties of cyanoalkyl biphenyl liquid crystals. Mol. Cryst. Liq. Cryst. **45**(1–2), 37–41 (1978). https://doi.org/10.1080/00268947808084998
15. R. Balamurugan, J.H. Liu, A review of the fabrication of photonic band gap materials based on cholesteric liquid crystals. React. Funct. Polym. **105**, 9–34 (2016). https://doi.org/10.1016/j.reactfunctpolym.2016.04.012
16. M.J. Cook, M.R. Wilson, Calculation of helical twisting power for liquid crystal chiral dopants. J. Chem. Phys. **112**(3), 1560–1564 (2000). https://doi.org/10.1063/1.480703
17. H. Kamberaj, M.A. Osipov, R.J. Low, M.P. Neal, Helical twisting power and chirality indices. Mol. Phys. **102**(5), 431–446 (2004). https://doi.org/10.1080/00268970410001670243
18. H. Kamberaj, R.J. Low, M.P. Neal, Molecular structure and helical twisting power. Ferroelectrics **315**(1), 183–196 (2005). https://doi.org/10.1080/00150190490509728
19. H.J. Gerritsen, R.T. Yamaguchi, A microwave analog of optical rotation in cholesteric liquid crystals. Am. J. Phys. **39**(8), 920–923 (1971). https://doi.org/10.1119/1.1986325
20. E. Sackmann, J. Voss, Circular dichroism of helically arranged molecules in cholesteric phases. Chem. Phys. Lett. **14**(4), 528–532 (1972). https://doi.org/10.1016/0009-2614(72)80256-2
21. R. Dreher, G. Meier, A. Saupe, Selective reflection by cholesteric liquid crystals. Mol. Cryst. Liq. Cryst. **13**(1), 17–26 (1971). https://doi.org/10.1080/15421407108083534
22. R. Dreher, G. Meier, Optical properties of cholesteric liquid crystals. Phys. Rev. A **8**(3), 1616 (1973). https://doi.org/10.1103/PhysRevA.8.1616
23. S.Y. Lu, L.C. Chien, A polymer-stabilized single-layer color cholesteric liquid crystal display with anisotropic reflection. Appl. Phys. Lett. **91**(13), 131119 (2007). https://doi.org/10.1063/1.2790499
24. X. Zhan, F.F. Xu, Z. Zhou, Y. Yan, J. Yao, Y.S. Zhao, 3D laser displays based on circularly polarized lasing from cholesteric liquid crystal arrays. Adv. Mater. **33**(37), 2104418 (2021). https://doi.org/10.1002/adma.202104418
25. M.F. Moreira, I.C.S. Carvalho, W. Cao, C. Bailey, B. Taheri, P. Palffy-Muhoray, Cholesteric liquid-crystal laser as an optic fiber-based temperature sensor. Appl. Phys. Lett. **85**(14), 2691–2693 (2004). https://doi.org/10.1063/1.1781363
26. Y. Han, K. Pacheco, C.W.M. Bastiaansen, D.J. Broer, R.P. Sijbesma, Optical monitoring of gases with cholesteric liquid crystals. J. Am. Chem. Soc. **132**(9), 2961–2967 (2010). https://doi.org/10.1021/ja907826z
27. R.C. Chambers, E.J. Bell, T.M. Records, A. Cherian, K. Ragan, B. Swartout, Cholesteric liquid crystal displays as optical sensors of barbiturate binding. Liq. Cryst. **34**(10), 1221–1226 (2007). https://doi.org/10.1080/02678290701658258
28. C.C. Li, H.Y. Tseng, C.W. Chen, C.T. Wang, H.C. Jau, Y.C. Wu, W.H. Hsu, T.H. Lin, Versatile energy-saving smart glass based on tristable cholesteric liquid crystals. ACS Appl. Energy Mater. **3**(8), 7601–7609 (2020). https://doi.org/10.1021/acsaem.0c01033
29. Z. Lan, Y. Li, H. Dai, D. Luo, Bistable smart window based on ionic liquid doped cholesteric liquid crystal. IEEE Photonics J. **9**(1), 1–7 (2017). https://doi.org/10.1109/JPHOT.2017.2653862
30. G. Chauhan, P. Malik, A. Deep, Morphological, dielectric, electro-optic and photoluminescence properties of TiO_2 nanoparticle enriched polymer stabilized cholesteric liquid crystals. J. Mol. Liq. **376**, 121406 (2023). https://doi.org/10.1016/j.molliq.2023.121406
31. A.K. Singh, P. Malik, Textural, electro-optical, dielectric and fluorescence studies of gold nanoparticle doped polymer-dispersed liquid crystals. Liq. Cryst. **49**(6), 864–874 (2022). https://doi.org/10.1080/02678292.2022.2027532
32. J. Zhang, Y. Zhang, J. Yang, X. Wang, Beyond color boundaries: pioneering developments in cholesteric liquid crystal photonic actuators. Micromachines **15**(6), 808 (2024). https://doi.org/10.3390/mi15060808
33. B. Gollapelli, S. Potu, R. Rajaboina, J. Vallamkondu, Optical anti-counterfeiting with cholesteric liquid crystal emulsions. Mater. Adv. **5**(18), 7113–7129 (2024). https://doi.org/10.1039/D4MA00604F
34. X. Liu, L. Qin, Y. Yu, Dynamic manipulation of photonic bandgaps in cholesteric liquid crystal microdroplets. Acta Phys.-Chim. Sin. **40**(5), 2305018 (2024). https://doi.org/10.3866/PKU.WHXB202305018
35. D.K. Yang, J.L. West, L.C. Chien, J.W. Doane, Control of reflectivity and bistability in cholesteric liquid crystal displays. J. Appl. Phys. **76**(2), 1331–1333 (1994). https://doi.org/10.1063/1.358518
36. J.K. Kim, S.H. Joo, J.K. Song, Reflective-emissive photoluminescent cholesteric liquid crystal display. Appl. Opt. **52**(34), 8280–8286 (2013). https://doi.org/10.1364/AO.52.008280

37. D.L. White, G.N. Taylor, New absorptive mode reflective liquid-crystal display device. J. Appl. Phys. **45**(11), 4718–4723 (1974). https://doi.org/10.1063/1.1663124
38. A.Y.G. Fuh, S.J. Ho, S.T. Wu, M.S. Li, Optical filter with tunable wavelength and bandwidth based on phototunable cholesteric liquid crystals. Appl. Opt. **53**(8), 1658–1662 (2014)
39. G. Nava, F. Ciciulla, F. Simoni, O. Iadlovska, O.D. Lavrentovich, L. Lucchetti, Heliconical cholesteric liquid crystals as electrically tunable optical filters. Liq. Cryst. **48**(11), 1534–1543 (2021). https://doi.org/10.1080/02678292.2021.1884911
40. A. Ryabchun, A. Bobrovsky, Cholesteric liquid crystal materials for tunable diffractive optics. Adv. Opt. Mater. **6**(15), 1800335 (2018). https://doi.org/10.1002/adom.201800335
41. T.J. White, S.A. Cazzell, A.S. Freer, D.K. Yang, L. Sukhomlinova, T. Kosa, B. Taheri, T.J. Bunning, Widely tunable photo invertible cholesteric liquid crystals. Adv. Mater. **23**(11), 1389–1392 (2011). https://doi.org/10.1002/adma.201003577
42. M.H. Saeed, J.A. Herman, A. Das, D.T. Kennedy, T.J. White, Inverse elastocaloric output in supramolecular liquid crystalline elastomers. ACS Mater. Lett. **7**(8), 2688–2694 (2025). https://doi.org/10.1021/acsmaterialslett.5c00331
43. G.W. Gray, D.G. McDonnell, New low-melting cholesterogens for electro-optical displays. Electron. Lett. **23**(11), 556–557 (1975). https://doi.org/10.1049/el:19750425
44. K.K. Vardanyan, D.M. Sita, R.D. Walton, W.M. Saidel, K.M. Jones, Cyanobiphenyl liquid crystal composites with gold nanoparticles. RSC Adv. **3**(1), 259–273 (2013). https://doi.org/10.1039/C2RA21220J
45. G. Lim, H. Kikuchi, S.K. Hong, Effect of cyanobiphenyl homologues on electro-optical properties. Polym. J. **46**(6), 337–341 (2014). https://doi.org/10.1038/pj.2013.98
46. S. Yadav, P. Malik, Effect of magnetic nanoparticles on blue phase liquid crystals. Opt. Mater. **122**, 111670 (2021). https://doi.org/10.1016/j.optmat.2021.111670
47. I. Chirtoc, M. Chirtoc, C. Glorieux, J. Thoen, Determination of the order parameter and its critical exponent for n CB (n= 5–8) liquid crystals from refractive index data. Liq. Cryst. **31**(2), 229–240 (2004). https://doi.org/10.1080/02678290310001642540
48. G. Singh, P. Malik, S. Kumar, M. Kumar, B. Vidhani, J. Dalal, R. Pal, Effect of alkyl chain length on the dielectric and electro-optical properties of graphene quantum dots doped cyanobiphenyl based nematic liquid crystals composites. J. Mol. Liq. **415**, 126370 (2024). https://doi.org/10.1016/j.molliq.2024.126370
49. M.H. Saeed, S. Zhang, L. Zhou, G. Chen, M. Wang, L. Zhang, D. Yang, H. Yang, Effects of rigid structures containing (meth) acrylate monomers and crosslinking agents with different chain length on the morphology and electro-optical properties of polymer-dispersed liquid crystal films. J. Mod. Opt. **67**(8), 682–691 (2020)
50. P. Malik, G. Chauhan, P. Kumar, A. Deep, Polymer concentration effects in confined ferroelectric liquid crystals. Liq. Cryst. **49**(14), 2008–2018 (2022). https://doi.org/10.1080/02678292.2022.2094006
51. Khushboo, A. Devi, P. Malik, H. Kumar, Thermodynamic and acoustical study of ZnO-nematic liquid crystals. J. Mol. Liq. **214**, 145–148 (2016). https://doi.org/10.1016/j.molliq.2015.11.025
52. I. Dierking, *Textures of Liquid Crystals* (John Wiley & Sons, 2003)
53. S. Havriliak, S. Negami, Complex plane analysis of α-dispersions in polymers. J. Polym. Sci. C Polym. Symp. **14**(1), 99–117 (1966). https://doi.org/10.1002/polc.5070140111
54. K.S. Cole, R.H. Cole, Dispersion and absorption in dielectrics. J. Chem. Phys. **9**(4), 341–351 (1941). https://doi.org/10.1063/1.1750906
55. S. Havriliak, S. Negami, Representation of dielectric relaxation processes. Polymer **8**, 161–210 (1967). https://doi.org/10.1016/0032-3861(67)90021-3
56. M. Kaur, P.K. Tripathi, B.P. Singh, K. Vikram, G. Singh, P. Malik, R. Manohar, S.J. Hwang, Morphology, dielectric, electro-optical and optical properties of diamond nanoparticle doped negative dielectric anisotropy liquid crystal. J. Mol. Liq. **417**, 126571 (2025). https://doi.org/10.1016/j.molliq.2024.126571
57. J. Thoen, G. Menu, Temperature dependence of the static relative permittivity of octylcyanobiphenyl (8CB). Mol. Cryst. Liq. Cryst. **97**(1), 163–176 (1983). https://doi.org/10.1080/00268948308073148
58. M. Walker, M.R. Wilson, Simulation insights into the role of antiparallel molecular association in the formation of smectic A phases. Soft Matter **12**(43), 8876–8883 (2016). https://doi.org/10.1039/C6SM01920J
59. K. Abe, A. Usami, K. Ishida, Y. Fukushima, T. Shigenari, Dielectric and fluorescence study of 5CB and 8CB. J. Korean Phys. Soc. **46**, 220–223 (2005)
60. S.P. Yadav, R. Manohar, S. Singh, Effect of TiO_2 nanoparticles on ionic behaviour. Liq. Cryst. **42**(8), 1095–1101 (2015). https://doi.org/10.1080/02678292.2015.1025872
61. P. Priscilla, A.K. Singh, P. Malik, S. Kumar, A.K. Gathania, J. Prakash, R. Castagna, D.E. Lucchetta, P. Malik, G. Singh, Effect of doping of organo-soluble carbon dots on ionic relaxation and conductivity of planar anchored

cyanobiphenyl based nematic liquid crystal. J. Mol. Struct. **1301**, 137403 (2024)
62. H. Verma, A. Lal, P.K. Singh, M.B. Pandey, R. Dabrowski, R. Dhar, Silver nanoparticles induced enhanced stability, dielectric anisotropy, and electro-optical parameters of a nematic liquid crystalline material 4-(trans-4-n-hexylcyclohexyl) isothiocyanatobenzene. J. Mol. Liq. **400**, 124503 (2024)
63. R.R. Deshmukh, A.J. Katariya, The complete morphological, electro-optical and dielectric study of dichroic dye-doped polymer-dispersed liquid crystal. Liq. Cryst. **41**(7), 960–975 (2014). https://doi.org/10.1080/02678292.2014.896051
64. P.G. de Gennes, J. Prost, *The Physics of Liquid Crystals* (Oxford University Press, 1993)
65. A. Shah, M.S. Sannaikar, S.R. Inamdar, B. Duponchel, R. Douali, D.P. Singh, Photoluminescence modulation in the graphene oxide dispersed 4-n-octyl-4'-cyanobiphenyl molecular system. J. Lumin. **226**, 117509 (2020). https://doi.org/10.1016/j.jlumin.2020.117509
66. C. David, V.D. Baeyens, Absorption and fluorescence spectra of 4-cyanobiphenyl and 4'-Alkyl-or 4'-Alkoxy-Substituted liquid crystalline derivatives. Mol. Cryst. Liq. Cryst. **59**(3–4), 181–196 (1980). https://doi.org/10.1080/00268948008071422
67. S.A. Oladepo, Temperature-dependent fluorescence emission of 4-cyano-4′-pentylbiphenyl and 4-cyano-4′-hexylbiphenyl liquid crystals and their bulk phase transitions. J. Mol. Liq. **323**, 114590 (2021). https://doi.org/10.1016/j.molliq.2020.114590
68. S. Inui, H. Kitaoka, Y. Eguchi, M. Yasui, T. Konno, S. Yamada, Design of Near-UV photoluminescent liquid-crystalline dimers: Roles of fluorinated aromatic ring position and flexible linker. Crystals **15**(10), 840 (2025). https://doi.org/10.3390/cryst15100840